JOURNAL OF THERMOPHYSICS AND HEAT TRANSFER
Vol. 14, No. 2, April–June 2000

Thermal Analysis During Continuous Casting Process Using Effective Heat Capacity Method

M. Ruhul Amin*
Montana State University, Bozeman, Montana 59717

A numerical analysis has been carried out to investigate the two-phase solidification process in continuous castings. An effective heat capacity method is used for this purpose. The radiation heat transfer at the mold metal interface was taken into account. The results of this method match well with the results obtained by analytical methods. The investigation included the ranges of mold cooling rate Bi_2, inlet temperature θ_0, and Peclet number Pe from 0.1–0.5, 1.2–2.0, and 0.1–1.0, respectively. A constant Stefan number Ste of 2.5 was used. It is observed that the solidification process is delayed with the increase of the withdrawal speed and with the increase of the liquid metal inlet temperature. With increased withdrawal speed, the region with temperature gradient moves downward. Steep axial temperature gradient was observed in the cast metal in the mold region.

Nomenclature

Bi = Biot number, hd/k_s
C = specific heat
d = half the width of the cast material; see Fig. 1
g = gravitational acceleration
h = heat transfer coefficient
h_r = radiation heat transfer coefficient
k = thermal conductivity
L = latent heat
P = pressure
Pe = Peclet number, $U_s d/\alpha_s$
Ste = Stefan number, $C_s(T_f - T_\infty)/L$
T = temperature
t = time
U_s = withdrawal speed
u = x component of velocity
v = y component of velocity
x, y = spatial coordinates; see Fig. 1
α = thermal diffusivity, $k/\rho C$
β = coefficient of volumetric expansion
ϵ = emissivity
θ = dimensionless temperature, $(T - T_\infty)/(T_f - T_\infty)$
μ = dynamic viscosity
ρ = density
σ = Stefan–Boltzmann constant

Subscripts

f = phase change
l = liquidus or liquid
m = mold
s = solidus or solid
0 = inlet
∞ = ambient

Introduction

ONE of the widely used important manufacturing processes for metals is continuous casting. This method offers several advantages that include 1) a dendritic but more dense and uniform microstructure (because of the uniform treatment in the mold) of the processed metal, 2) low unit labor cost because of the essentially automatic process, and 3) simple and inexpensive molds. A basic continuous casting process is shown in Fig. 1. It involves two steps. The molten metal first passes through a mold, which is usually cooled by water, followed by a high cooling rate downstream. As a result, the molten metal solidifies through a phase change, and the solidified ingot is withdrawn at a uniform velocity. This process is similar to some other manufacturing techniques such as optical and glass fiber drawing, wire drawing, hot rolling, plastic extrusion, and Czochralski crystal growing. Phase change problems involving melting or solidification are referred to as the free boundary or the moving boundary problems. The solution of this type of problem is inherently difficult because, at the solid–liquid interface, there is a discontinuity in the temperature gradient (heat flux) due to the liberation or absorption of energy (latent heat). As a result, the solid–liquid interface moves with time, the location of which is not known a priori; it must be followed as part of the solution process.

The large volume of literature in the melting and solidification technology indicates the growing research interest in this area among mathematicians and engineers. The topic has obvious practical importance in a wide range of applications. The heat transfer mechanism in a phase change problem is of sufficient complexity to obtain an analytical solution without oversimplification. For example, in a solidification process, the superheat in the melt and the latent heat of fusion liberated at the solid–liquid interface encounters a series of thermal resistances. The liberated energy is transferred across the solidified metal, metal–mold interface, and the mold. A controlled extraction of heat in a process involving phase change is very important because it affects the thermal stress and the quality of the final product. However, the heat transfer mechanism in such a process is complex and not yet fully understood. With the arrival of high-speed computing technology, various numerical methods have provided the alternatives to the often oversimplified analytical solutions. A very complex problem with difficult boundary conditions can be solved numerically in a reasonable amount of time and cost by selecting a correct mathematical model describing the physical problem and coupling with an appropriate algorithm.

A close relationship exists between the mechanical behavior of polycrystalline metallic materials, that is, castings, ingots, etc., and their microstructural soundness. The structural perfection of a casting or ingot depends on many parameters, such as grain size and growth, temperature gradient at the solid–liquid interface, and the rate of thermal cooling. Interaction among these parameters is mainly controlled by the cooling rate. The heat extraction rate in the solidifying process, by different cooling methods, produces variations of microstructure as well as metallurgical and mechanical properties. The solidification process is of great importance because, for low melting point metals, it is the most economical method of forming a component. The understanding of thermodynamics,

Received 19 July 1999; revision received 22 November 1999; accepted for publication 22 November 1999.

*Associate Professor, Department of Mechanical and Industrial Engineering; ramin@me.montana.edu.

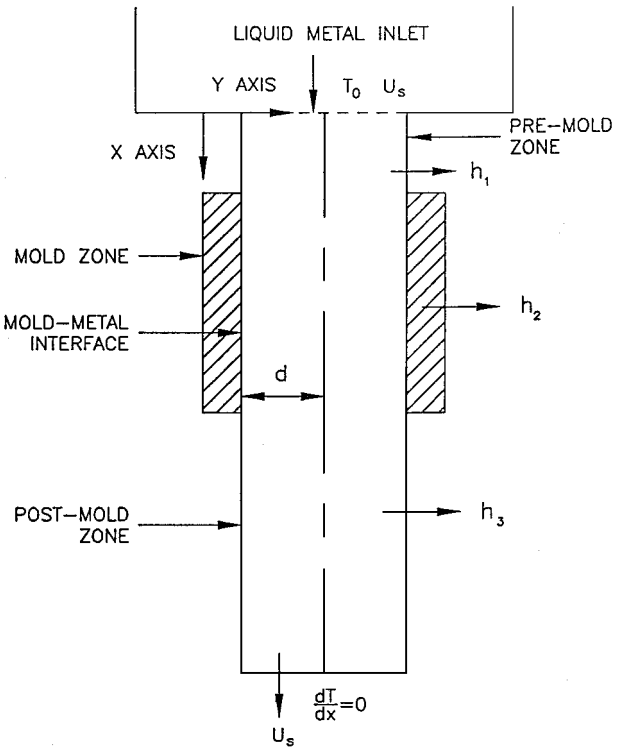

Fig. 1 Investigated geometry.

phase-transformation kinetics, transport process, and solid mechanics is vital to encompass any solidification process.

An earlier evaluation by Sparrow et al.[1] of the previous work in this area noted that most of the analyses assumed conduction heat transfer was the only transport mechanism of significant importance. Obviously, such an assumption is not applicable in all problems. When the molten metal flows under an imposed pressure gradient, forced convective flow occurs. Similarly, buoyancy-induced flow may occur in the molten metal pool due to nonuniform temperature distribution. Thus, for a large class of problems, the assumption of only conduction heat transfer is not valid; the influence of convective flow must also be considered in many phase change transport processes. The review paper by Viskanta[2] discusses recent advances in the understanding of melting and solidification mechanisms in metals and alloys. The importance of the convective flows, in particular, the buoyancy induced flows, is discussed. Recently, Jaluria[3] reviewed the works on the transport mechanisms from continuously moving materials undergoing thermal processing.

Investigators such as Blackwell and Ockendon,[4] Szekely et al.,[5] and DeBellis and LeBeau[6] have performed analytical and numerical studies on continuous casting problems. Since its inception, the so-called enthalpy model (single-region approach) has been widely used to solve phase change problems. Bennon and Incropera[7] have applied the enthalpy method to a solidification flow process in a channel. Among others, Chidiac et al.[8] have used the enthalpy method in the transient continuous casting process.

A continuous casting process involves two distinct cooling mechanisms. Molten metal first flows through a mold, where cooling is done by circulating water through the mold. By the time the moving metal leaves the mold, depending on the cooling rate, the molten metal either solidifies completely or at least a solid crust develops on the outer periphery. Downstream, in the submold region, the moving metal is cooled more rapidly by spray cooling. Roy Choudhury and Jaluria[9] performed a numerical study of the forced convection cooling of a continuously moving cylindrical rod. Both aiding and opposing flows of the cooling fluid were considered. The heat transfer in the mold region was not considered in their study. In another study, Kang and Jaluria[10] used the enthalpy method to model the thermal phenomena in a continuous casting process. They considered the premold, mold, and submold regions in their study. Recently, Aboutalebi et al.[11] performed a numerical study of coupled turbulent flow and solidification for a continuously moving slab caster. By the using of the enthalpy–porosity method, the authors considered both the mold and submold regions.

It is seen from the preceding discussion that none of the studies have considered the effects of mold thickness and the conjugate heat transfer in the mold region for a continuous casting process. A recent study by Viswanath and Jaluria[12] on solidification in an enclosed region shows the importance of considering the conjugate heat transfer in the mold region. Their study also shows the importance of considering the effects of mold thickness and aspect ratio. During solidification, most of the metals shrink. As a result, an air gap is created between the metal and mold. The heat transfer coefficient at this interface is nonlinear. Kim et al.,[13] Huang et al.,[14] and Piwonka and Berry[15] have done some exploration on the variable convective and radiative heat transfer at the metal–mold interface. This aspect needs to be considered in the analysis of continuous casting.

In the present study, an effective heat capacity method is used for the analysis of the two-phase solidification in continuous casting process. This method has successfully been used in liquid–solid phase change problems by Gartling.[16] The radiation heat transfer at the metal–mold interface is taken into account. The conduction heat transfer effects in the mold and solidified metal were considered. Thus, the effects of the conjugate heat transfer were considered. Figure 1 shows the investigated geometry, where different heat transfer rates were assigned in the premold, mold, and postmold regions. Liquid metal enters the mold at a constant inlet temperature, and the solidified metal is withdrawn at a specified speed. Successful implementation of the effective heat capacity method along with the mold–metal interface radiation heat transfer is achieved in this study.

Mathematical Formulation

Modeling Assumptions

The geometry shown in Fig. 1 is used for the present study. The governing equations are simplified by the following assumptions:

1) The geometry is limited to two dimensions.
2) The fluid is Newtonian.
3) The flow is laminar, incompressible, and within Boussinesq approximation.
4) The change in material density upon the change of the phase is negligible.
5) The fluid is radiatively nonparticipating.
6) The effects of latent heat will be adequately accounted for through appropriate modification of the specific heat.
7) Viscous dissipation and compressive work are negligibly small.

Governing Equations

Based on the preceding assumptions, the conservation of mass, momentum, and energy equations in dimensional form can be written as

$$\frac{\partial u}{\partial x}+\frac{\partial v}{\partial y}=0 \tag{1}$$

$$\rho\frac{\partial u}{\partial t}+\rho u\frac{\partial u}{\partial x}+\rho v\frac{\partial u}{\partial y}=-\frac{\partial P}{\partial x}+\mu\left[\frac{\partial^2 u}{\partial x^2}+\frac{\partial^2 u}{\partial y^2}\right]+\rho g\beta(T-T_\infty) \tag{2}$$

$$\rho\frac{\partial v}{\partial t}+\rho u\frac{\partial v}{\partial x}+\rho v\frac{\partial v}{\partial y}=-\frac{\partial P}{\partial y}+\mu\left[\frac{\partial^2 v}{\partial x^2}+\frac{\partial^2 v}{\partial y^2}\right] \tag{3}$$

$$\rho C\left[\frac{\partial T}{\partial t}+u\frac{\partial T}{\partial x}+v\frac{\partial T}{\partial y}\right]=k\left[\frac{\partial^2 T}{\partial x^2}+\frac{\partial^2 T}{\partial y^2}\right] \tag{4}$$

where the density ρ is constant throughout solid and liquid. The so-called side effects of assuming constant density is discussed later in

this paper. Following Bonacina et al.,[17] the specific heat and thermal conductivity in the energy equation are expressed as

$$C = \begin{cases} C_s & \text{for} \quad T \prec T_f - \Delta T \\ L/2\Delta T + (C_s + C_l)/2 & \text{for} \quad T_f - \Delta T \leq T \leq T_f + \Delta T \\ C_l & \text{for} \quad T \succ T_f + \Delta T \end{cases} \tag{5}$$

$$k = \begin{cases} k_s & \text{for} \quad T \prec T_f - \Delta T \\ k_s + [(k_l - k_s)/2\Delta T][T - (T - \Delta T)] & \text{for} \\ \qquad\qquad T_f - \Delta T \leq T \leq T_f + \Delta T \\ k_l & \text{for} \quad T \succ T_f + \Delta T \end{cases} \tag{6}$$

where $2\Delta T$ is the small temperature difference across the solidification temperature T_f.

In the continuity and momentum equations, liquid metal properties are used. When the temperature reaches the solidification temperature T_f, a very high value of fluid viscosity (of the order of 10^{20}) is assigned to solve essentially a very stiff momentum equation. This process eliminates continuity and momentum equations when solidification is achieved. The only governing equation that controls the heat transfer process at that state is the energy equation. At this state the velocity vector in the energy equation for the cast material is assigned the constant withdrawal speed U_s for the x component and zero value for the y component. The relevant boundary conditions for the governing equations are shown in Fig. 1. As discussed by Bonacina et al.,[17] the phase boundary conditions are also satisfied by the use of Eqs. (5) and (6). This is the essence of the equivalent heat capacity method used in the present analysis.

Liquid metal shrinks on solidification, resulting in an air gap between the mold and the solidified metal. The mold–metal interfacial heat transfer is taken into account by applying a radiative heat transfer coefficient at the interface.

The radiative heat transfer coefficient is expressed as

$$h_r = \frac{\sigma(T_m^2 + T_s^2)(T_m + T_s)}{1/\varepsilon_m + 1/\varepsilon_s - 1} \tag{7}$$

In Eq. (7), T_m and T_s are the temperatures of the mold surface and solidified metal, at a particular location, respectively. These temperatures change with time until steady state is reached. The value of h_r is calculated internally in the code for each iteration using the latest values of the temperature.

Numerical Procedure

Code Description

The dimensional governing equations for the present study were solved by using the finite element code NACHOS II, developed by Gartling.[18] It is a general-purpose finite element code designed to solve the two-dimensional continuity, momentum, and energy equations for both steady state and transient problems. A detail description of the code has been documented elsewhere.[18] For the purpose of the present two-phase problem, substantial modification of code has been made to incorporate the equivalent heat capacity method. Note that in the current work, the material used was pure aluminum; as such, no mushy zone was present. However, for alloys a mushy zone exists in between the solidified and the liquid regions. In the present numerical method, the mushy zone for alloy solidification can be incorporated by treating the entire computational domain as a porous medium with some temperature-dependent constraints so that the advection term related to porous flow is used or not used. If the advection term related to the porous flow is not used, then the governing equation is the same as for the liquid flow case. The value of permeability required to be used in the porous flow equation is zero when the medium is solid. When the medium is liquid, permeability is infinite. Appropriate values for permeability can be used to model the mushy zone. Another option could be to use temperature-dependent viscosity in the current method to model the mushy zone during alloy solidification.

The finite element grids used by NACHOS II were arranged such that more elements were packed into regions of large gradients of velocity and/or temperature. The grids were generated by the internal grid generator of the code. Note that the grid generator of the code can generate nine grid points for each element, four at the corner points of the element, one at the center of each side of the element (total of four), and one at the center of the element. For the present geometry, after the grid independency test, 374 elements were used, which resulted 1617 nodes. The dimensional transient forms of the governing equations were solved. Results are obtained in terms of primitive variables. All computations were performed on a Cray C90 supercomputer using a FORTRAN 77 compiler under the UNIX operating system.

For convergence criteria, NACHOS II uses the discrete norms defined by

$$d_{n+1}^U = \frac{1}{U_{\max}} \left[\sum_{j=1}^{N} (U_j^{n+1} - U_j^n)^2 \right]^{\frac{1}{2}}$$

$$d_{n+1}^T = \frac{1}{T_{\max}} \left[\sum_{j=1}^{N} (T_j^{n+1} - T_j^n)^2 \right]^{\frac{1}{2}} \tag{8}$$

In Eq. (8), the subscript max indicates the maximum value of the variable found at the $(n + 1)$th iteration, and N is the total number of nodal points. For convergence, the following inequalities were satisfied:

$$d_{n+1}^U \leq \phi^U, \qquad d_{n+1}^T \leq \phi^T \tag{9}$$

where the tolerance parameter ϕ was set to 10^{-4}.

Computational Models

Because of the symmetry of the present geometry along the centerline, half of the geometry shown in Fig. 1 was used for the numerical computation. To set the required fluid flow and heat transfer conditions using convenient parameters, the nondimensional form of the governing equations and boundary conditions were used. The definitions of the various nondimensional parameters used to set the conditions of the present problem are listed in the nomenclature section. The withdrawal speed is represented in nondimensional form as the Peclet number *Pe*. The inlet temperature of the liquid metal is expressed in nondimensional form as θ_0. Other important nondimensional parameters are Stefan number *Ste* and Biot number *Bi*. The length scale is nondimensionalized by half of the casting width d.

Results and Discussion

As discussed earlier, the present numerical investigation was performed by using the general purpose finite element code NACHOS II. This code has been well tested with the solution of many benchmark problems involving free and force convection heat transfers in clear fluid and in porous media. Results of these testings, relevant to the present investigation, are reported by Gartling.[16,19] In these papers, comparisons were made for several problems, including forced convection in tubes involving variable viscosity and wall conduction, forced convection with phase change including the effect of conduction through the solid phase, and buoyancy-driven flows in enclosures.

To demonstrate the numerical accuracy of the present method, comparisons were made with the results of other analyses. Figure 2 shows a comparison of the analytical results obtained by Siegel[20] with the current method. In this comparison, the length of the insulated mold was taken to be equal to $3d$. The solid lines in Fig. 2 indicate the location and the shape of the solid–liquid interface obtained

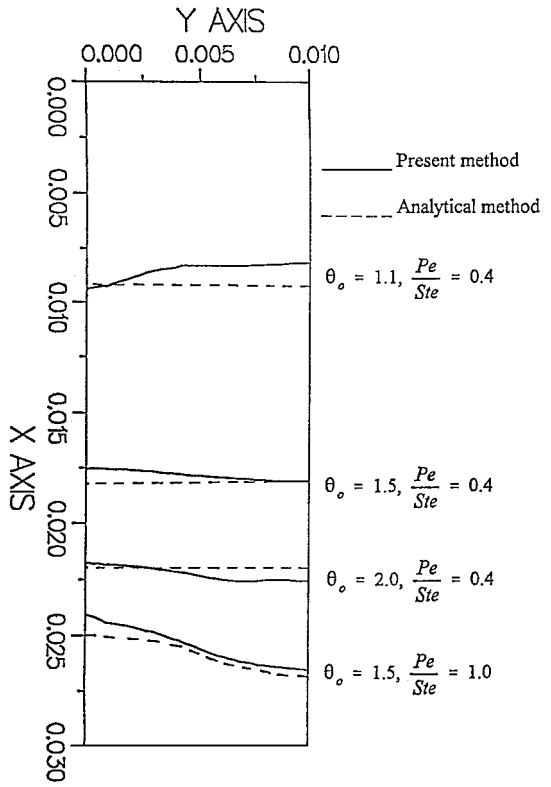

Fig. 2 Comparison with the results of analytical solution from Siegel.[20]

by the present method, and the dotted lines indicate the interface obtained by Siegel. Good agreement can be seen. The discrepancy is because Siegel[20] assumed that the cast material is withdrawn very slowly. Whereas in the present method, the cast material has a finite withdrawal speed. Siegel also assumed that the latent heat of fusion is removed locally along the solid–liquid interface. Figure 3 shows the isotherms obtained by the present method (without the interface radiation and the conduction heat transfer in the mold) for a case with $Pe = 0.3$, $Ste = 2.5$, $\theta_0 = 1.2$, $Bi_1 = 0.0$, $Bi_2 = 0.1$, and $Bi_3 = 0.5$. This is for comparison with the corresponding case obtained by enthalpy method and reported by Kang and Jaluria.[10] Figure 3 is to be compared with Fig. 10d of Kang and Jaluria's paper. Good agreement can be seen, except that the current method does not have mushy zone. Additional cases were run to compare a few other cases from Kang and Jaluria's paper. Good agreement was found in those cases as well. These comparisons and other tests by Gartling[16] gave us the confidence that the current equivalent heat capacity method has been successfully employed for the numerical analysis of two-phase continuous casting problems.

For the purpose of the present analysis, an aspect ratio of 20 is used. As reported by Kang and Jaluria,[10] this aspect ratio is found to be adequate to obtain a developed temperature distribution with the present boundary conditions. The premold, mold, and postmold nondimensional distances used in the current research were 2.0, 8.0, and 10.0, respectively. A mold aspect ratio of 32 is used. Aluminum and copper are used as the casting and mold materials respectively. The nondimensional heat transfer coefficients at the premold, mold, and postmold zones are expressed as Bi_1, Bi_2, and Bi_3, respectively. For the present analysis, the premold zone was assumed to be insulated, $Bi_1 = 0$. The values of Bi_2 were varied from 0.1 to 0.5. The postmold heat transfer coefficient was fixed to a value of $Bi_3 = 0.5$.

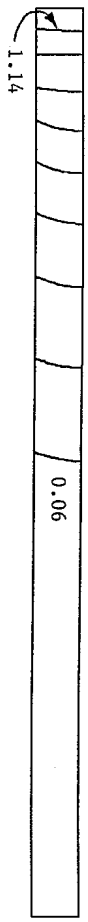

Fig. 3 Isotherms for a case with $Ste = 2.5$, $Pe = 0.3$, $\theta_0 = 1.2$, $Bi_1 = 0.0$, $Bi_2 = 0.1$, and $Bi_3 = 0.5$.

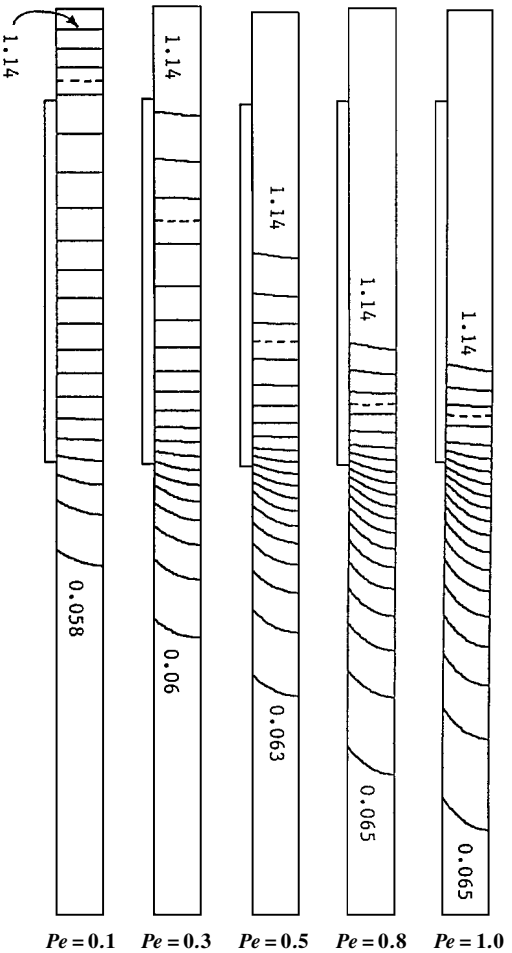

Fig. 4 Effect of the withdrawal speed: $Ste = 2.5$, $\theta_0 = 1.2$, $Bi_1 = 0.0$, $Bi_2 = 0.1$, and $Bi_3 = 0.5$.

A constant Stefan number *Ste* of 2.5 was used throughout this study. The nondimensional inlet temperature θ_0 of liquid aluminum was varied from 1.2 to 2.0. The range of Peclet number *Pe* used was 0.1–1.0. To study the effects of the withdrawal speed, inlet temperature, and the cooling rate, nondimensional temperature distributions are shown in Figs. 4–6. The highest and the lowest values of the nondimensional temperature θ are also shown in Figs. 4–6. The dotted lines in Figs. 4–6 indicate the location and the shape of the solid–liquid interface.

Figure 4 shows the effects of the withdrawal speed. The nondimensional form of the withdrawal speed is expressed in terms of Peclet number *Pe*. The mold cooling rate Bi_2 and the inlet temperature θ_0 are kept constant at 0.1 and 1.2, respectively. Note that, as expected, for the same cooling rate and inlet temperature of the liquid metal, the region with temperature gradients gradually moves from the leading zone to the trailing zone. At lower withdrawal speed, the lower portion of the casting is isothermal, and at higher withdrawal speed, the upper portion becomes isothermal (after reaching a steady-state condition). The solid–liquid interface (shown by the dotted line) also moves downward with increasing withdrawal speed. This means that the solidification process starts earlier for a slower withdrawal speed. The solid–liquid interfacial isotherm shows a flat interface. From the values of isotherms in Fig. 4, it can be seen that with the increase in withdrawal speed, the steady-state temperature of the lower portion of the casting material also increases.

The effects of the inlet temperature of the liquid metal during the continuous casting process are shown in Fig. 5. Note that the locations of the temperature gradients remain almost unaltered. However, as expected, the physical values of the temperature of the region increase with the increasing values of θ_0. Note from Fig. 5 that with

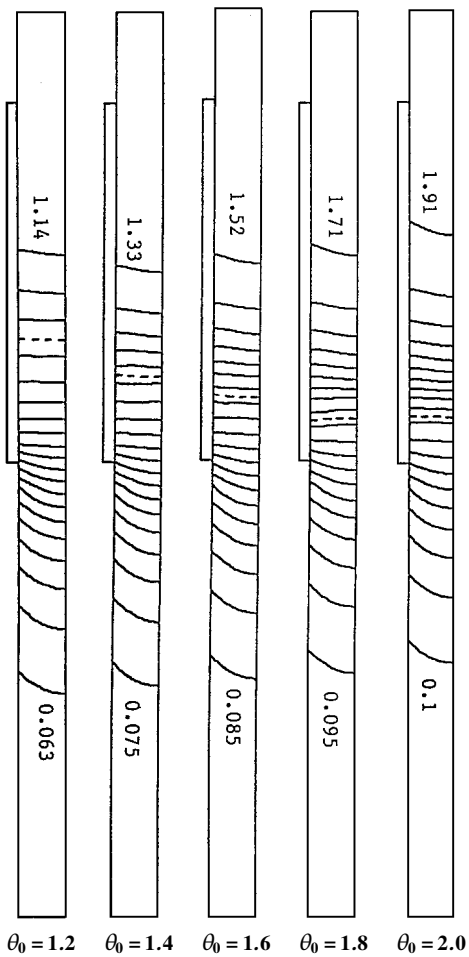

Fig. 5 Effect of the inlet temperature of the liquid metal: *Ste* = 2.5, *Pe* = 0.5, $Bi_1 = 0.0$, $Bi_2 = 0.1$, and $Bi_3 = 0.5$.

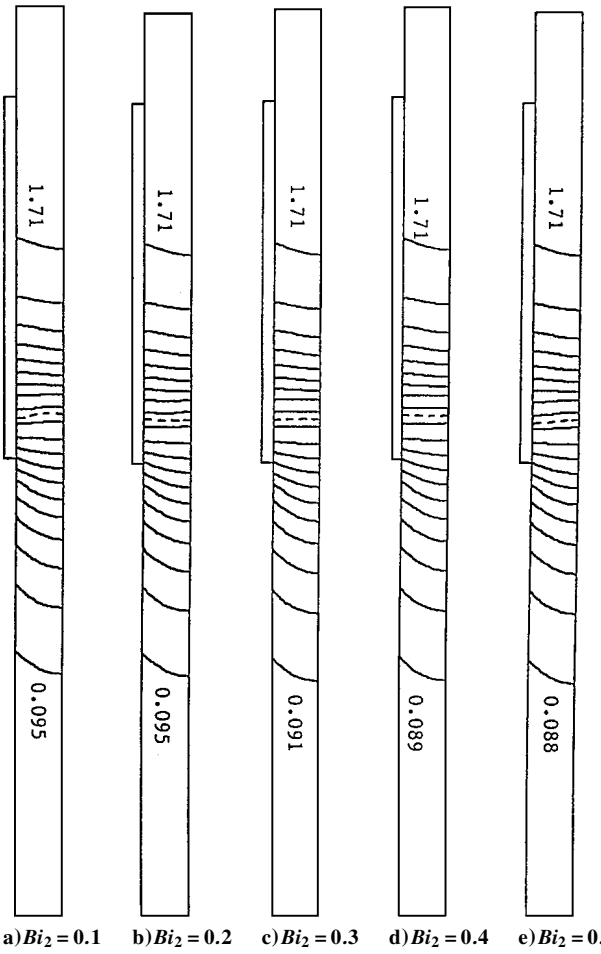

Fig. 6 Effect of the mold cooling rate: *Ste* = 2.5, *Pe* = 0.5, $\theta_0 = 1.8$, $Bi_1 = 0.0$, $Bi_3 = 0.5$.

the increase of θ_0, the solid–liquid interface moves downstream. This is expected because, with the increasing inlet temperature of the liquid metal, the solidification will start farther downstream (delay in solidification). With the increasing values of the liquid inlet temperature, the values of the temperature across the region also increase. At the current withdrawal speed, $Pe = 0.5$, it can be seen that the leading and the trailing regions of the cast material become isothermal after the steady-state condition is achieved.

Figure 6 shows the effects of the cooling rate in the mold region during the solidification process. Note that with the increase in the cooling rate, the temperature at the downstream decreases. For the present values of premold and postmold cooling rates, the location of the solidification front does not change much with the mold cooling rate. The temperature distribution above the solidification region remains the same for different cooling rates. From the temperature distribution of Fig. 6, it can also be seen that the highest value of the temperature θ is almost the same in all of the cases, but the lowest value of θ decreases with the increase of the cooling rate. The qualitative nature of the temperature distribution remains the same for various cooling rates.

The nondimensional axial temperature distributions along the outer surface of the cast material ($0 \leq x \leq 20$ and $y = 0.25$) for a case with $Ste = 2.5$, $Pe = 0.5$, $\theta_0 = 1.8$, and $Bi_2 = 0.3$ are shown in Fig. 7. Note that the outer surface temperature of the cast material starts at $\theta = 1.8$ (inlet temperature of the liquid metal for this case) and gradually decreases to a value of $\theta \approx 0.009$ at the lower region of the cast material. The temperature of the premold region ($0 \leq x \leq 2$) is high because there is no cooling in this region. This region is kept insulated in the current study. A nonzero value of θ at the lower region indicates that the solidified metal is still at a temperature higher than the ambient temperature ($\theta = 0$, for ambient temperature) after the steady-state condition is reached. Inspection

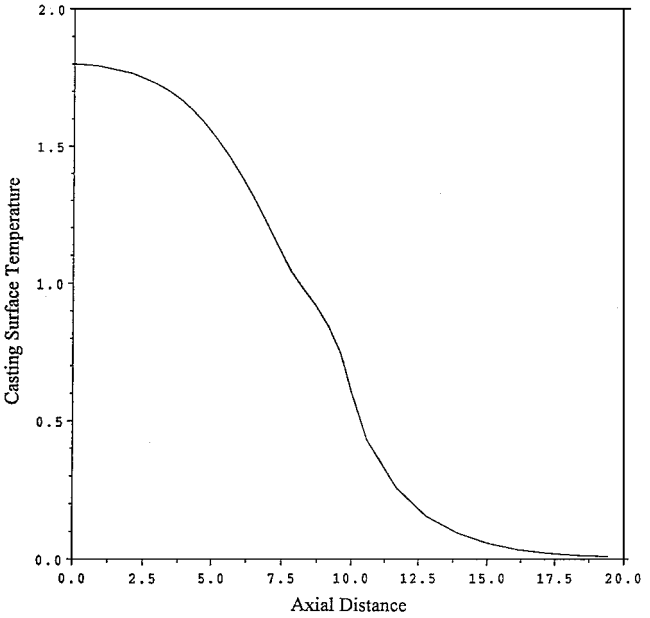

Fig. 7 Nondimensional axial temperature distribution: $Ste = 2.5$, $Pe = 0.5$, $\theta_0 = 1.8$, $Bi_1 = 0.0$, $Bi_2 = 0.3$, and $Bi_3 = 0.5$.

of the temperature between $2 \leq x \leq 10$ (mold region) shows that a very steep temperature gradient exists. This is expected, because of the high cooling rate in the mold region. From the casting temperature, it can also be seen that at steady state, the solid–liquid interface ($\theta = 1$) is at a location $x \approx 8$. This is consistent with the observation of the isotherms for this case, which are shown in Fig. 6c. Axial temperature distributions along axes away from the outer surface of the cast material show similar trend.

As discussed earlier, a radiation boundary condition was applied at the metal mold interface. However, inspection of the temperature distribution at the interface revealed minimal difference in the temperature. As such, insignificant effect due to radiation was observed. This is because in the current analysis the density of the metal is considered to be constant; hence, the shrinkage at the metal–mold interface actually does not exist. Therefore, the thermal resistance at the interface, due the shrinkage of the solidified metal, was not considered. The absence of such resistance due to the air gap might be the reason for such an insignificant change of temperature at the interface. A more accurate method of handling this region would be to incorporate thermal contact conductance between the metal and the mold. Further investigation on this issue is warranted, and the work is in progress as of this writing.

Conclusions

A finite element method was used to study the two-phase solidification process in continuous castings. Two-dimensional governing equations were solved using the effective heat capacity method. The mold–metal interface radiation heat transfer effects were taken into account. The main objective of this study was to demonstrate the successful implementation of the interface radiation heat transfer and the use of the effective heat capacity method for the numerical analysis of the continuous casting process. Good agreement with the results of the analytical method was obtained. The results from other numerical methods were also compared. The current method can be used successfully for other phase change processes in moving materials. These processes include crystal growing, plastic extrusion, glass fiber drawing, etc. Non-Newtonian fluids can be modeled easily by incorporating temperature-dependent viscosity, and the current code is equipped with this capability.

It is observed that with the increase of the withdrawal speed, the solid–liquid interface moves downward. This indicates a delay in the start of the solidification process. Other studies have observed similar trends. With the increase of the withdrawal speed, the region with the temperature gradients gradually moves from the leading zone to the trailing zone. As expected, it was observed that the solidification process starts farther downstream with the increase of the inlet temperature of the liquid metal at the mold entrance. After the steady-state condition is achieved, isothermal regions appear. These regions could be at the leading zone (all liquid region), or at the trailing zone (all solid region), or both. The exact location depends on the boundary conditions, such as liquid metal inlet temperature, mold cooling rate, and the withdrawal speed. For the ranges of the parameters investigated, it is observed that for various cooling rates at the mold region (with the other boundary conditions fixed), the steady-state temperature distribution above the solid–liquid interface remains almost unaltered. Past the interface, the temperature distribution changes with the cooling rate. Observation of the axial temperature distribution reveals that a steep temperature gradient exists at the mold region.

Acknowledgments

The author acknowledges the financial support for this study from MONTS, the National Science Foundation–Experimental Program to Stimulate Competitive Research at Montana State University. The numerical computations were performed on the Cray C90 machine at the Pittsburgh Supercomputer Center (PSC). The PSC supercomputing grant is also greatly appreciated.

References

[1] Sparrow, E. M., Patankar, S. V., and Ramadhyani, S., "Analysis of Melting in the Presence of Natural Convection in the Melt Region," *Journal of Heat Transfer*, Vol. 99, No. 4, 1977, pp. 520–526.

[2] Viskanta, R., "Heat Transfer During Melting and Solidification of Metals," *Journal of Heat Transfer*, Vol. 110, No. 4(B), 1988, pp. 1205–1219.

[3] Jaluria, Y., "Transport from Continuously Moving Materials Undergoing Thermal Processing," *Annual Review on Heat Transfer*, Vol. 4, 1992, pp. 187–245.

[4] Blackwell, J. H., and Ockendon, J. R., "Exact Solution of a Stefan Problem Relevant to Continuous Casting," *International Journal of Heat and Mass Transfer,* Vol. 25, No. 7, 1982, pp. 1059–1060.

[5] Szekely, J., Evans, J. W., and Brimacombe, J. K., "Modeling of the Continuous Casting of Steel," *The Mathematical and Physical Modeling of Primary Metals Processing Operations*, Wiley-Interscience, New York, 1988, pp. 197–227.

[6] DeBellis, C. L., and LeBeau, S. E., "A Verified Thermal Model for Continuous Casting Process," *Heat Transfer in Manufacturing and Materials Processing*, edited by R. K. Shah, American Society of Mechanical Engineers, Fairfield, NJ, 1989, pp. 105–111.

[7] Bennon, W. D., and Incropera, F. P., "A Continuum Model for Momentum, Heat and Species Transport in Binary Solid–Liquid Phase Change Systems—I. Model Formulation," *International Journal of Heat and Mass Transfer*, Vol. 30, No. 10, 1987, pp. 2161–2170.

[8] Chidiac, S. E., Samarasekera, I. V., and Brimacombe, J. K., "A Numerical Method for Analysis of Phase Change in the Continuous Casting Process," *Numiform 89, Proceedings of 3rd International Conference on Numerical Methods in Industrial Forming Process*, edited by E. C. Thompson, R. D. Wood, O. C. Zienkiewick, A. Samuelson, and A. A. Balkema, 1989, pp. 121–128.

[9] Roy Choudhury, S., and Jaluria, Y., "Forced Convective Heat Transfer from a Continuously Moving Heated Cylindrical Rod in Materials Processing," *Journal of Heat Transfer*, Vol. 116, No. 3, 1994, pp. 724–734.

[10] Kang, B. H., and Jaluria, Y., "Thermal Modeling of the Continuous Casting Process," *Journal of Thermophysics and Heat Transfer*, Vol. 7, No. 1, 1993, pp. 139–147.

[11] Aboutalebi, M. R., Hasan, M., and Guthrie, R. I. L., "Numerical Study of Coupled Turbulent Flow and Solidification for Steel Slab Casters," *Numerical Heat Transfer*, Pt. A, Vol. 28, No. 3, 1995, pp. 279–297.

[12] Viswanath, R., and Jaluria, Y., "Numerical Study of Conjugate Transient Solidification in an Enclosed Region," *Numerical Heat Transfer*, Part A, Vol. 27, No. 5, 1995, pp. 519–536.

[13] Kim, W. S., Ozisik, M. N., and Hector, L. G., Jr., "Inverse Problem of 1D Solidification for Determining Air-Gap Resistance to Heat Flow During Metal Casting," 22nd International Center for Heat and Mass Transfer International Symposium on Manufacturing and Material Processing, Dubrovnik, Yugoslavia, Aug. 1990.

[14] Huang, C. H., Ozisik, M. N., and Sawaf, B., "Conjugate Gradient Method for Determining Unknown Contact Conductance During Metal Casting," *International Journal of Heat and Mass Transfer*, Vol. 35, No. 7, 1992, pp. 1779–1786.

[15]Piwonka, T. S., and Berry, J. T., "Heat Transfer at the Mold/Metal Interface in Investment Castings," *41st Annual Technical Meeting: Investment Casting Institute*, Investment Casting Inst., Dallas, TX, 1993, pp. 15:1–15:17.

[16]Gartling, D. K., "Finite Element Analysis of Convective Heat Transfer Problems with Change of Phase," *Computer Methods in Fluids*, edited by K. Morgan, C. Taylor, and C. Brebbia, Pentech, London, 1980, pp. 257–284.

[17]Bonacina, C., Comini, G.,. Fasano, A., and Primicerio, M., "Numerical Solution of Phase-Change Problems," *International Journal of Heat and Mass Transfer*, Vol. 16, No. 10, 1973, pp. 1825–1832.

[18]Gartling, D. K., "NACHOS II—A Finite Element Computer Program for Incompressible Flow Problems, Part I—Theoretical Background," Sandia Labs., SAND86-1816, UC-32, Albuquerque, NM, 1987.

[19]Gartling, D. K., "Convective Heat Transfer Analysis by the Finite Element Method," *Computational Methods in Applied Mechanical Engineering*, Vol. 12, 1977, pp. 365–382.

[20]Siegel, R., "Two-Region Analysis of Interface Shape in Continuous Casting with Superheated Liquid," *Journal of Heat Transfer*, Vol. 106, No. 3, 1984, pp. 506–511.